www.nature.com/aps

Acta Pharmacologica Sinica

ARTICLE

Caspase-11/4 and gasdermin D-mediated pyroptosis contributes to podocyte injury in mouse diabetic nephropathy

Qian Cheng[1], Jing Pan[1], Zhuan-li Zhou[1], Fan Yin[1], Hong-yan Xie[1], Pan-pan Chen[1], Jing-yao Li[1], Pei-qing Zheng[1], Li Zhou[1], Wei Zhang[1], Jun Liu[1] and Li-min Lu[1]

Diabetic nephropathy (DN) is characterized by sterile inflammation with continuous injury and loss of renal inherent parenchyma cells. Podocyte is an essential early injury target in DN. The injury and loss of podocytes are closely associated with proteinuria, the early symptom of renal injury in DN. However, the exact mechanism for podocyte injury and death in DN remains ambiguous. In this study we investigated whether pyroptosis, a newly discovered cell death pathway was involved in DN. Diabetic mice were generated by high-fat diet/STZ injections. We showed that the expression levels of caspase-11 and cleavage of gasdermin D (GSDMD-N) in podocytes were significantly elevated, accompanied by reduced expression of podocyte makers nephrin and podocin, loss and fusion in podocyte foot processes, increased inflammatory cytokines NF-κB, IL-1β, and IL-18, macrophage infiltration, glomerular matrix expansion and increased urinary albumin to creatinine ratio (UACR). All these changes in diabetic mice were blunted by knockout of caspase-11 or GSDMD. Cultured human and mouse podocytes were treated with high glucose (30 mM), which significantly increased the expression levels of caspase-11 or caspase-4 (the homolog of caspase-11 in human), GSDMD-N, NF-κB, IL-1β, and IL-18, and decreased the expression of nephrin and podocin. Either caspase-4 or GSDMD knockdown by siRNA significantly blunted these changes. In summary, our results demonstrate that caspase-11/4 and GSDMD-mediated pyroptosis is activated and involved in podocyte loss under hyperglycemia condition and the development of DN.

Keywords: diabetic nephropathy; podocyte; caspase-11; gasdermin-D; pyroptosis

Acta Pharmacologica Sinica (2021) 42:954–963; https://doi.org/10.1038/s41401-020-00525-z

INTRODUCTION

Diabetic nephropathy (DN) is a severe complication of diabetes. With the increasing incidence of diabetes, DN has become an important pathogenic factor for the development of chronic kidney disease [1]. Approximately 30%–40% of end-stage kidney disease patients worldwide are diabetic patients [2]. The early indications of DN include proteinuria, glomerular mesangial matrix expansion, basement membrane (GBM) thickening and podocyte injury [3, 4]. As highly specialized differentiated cells, podocytes compose the outermost layer of the glomerular filtration barrier. Therefore, podocyte injury is strictly associated with the development of proteinuria [5]. Due to the limited regenerative ability of podocytes, podocyte damage, and loss may lead to the destruction of the glomerular filtration membrane [6, 7]. The degree of podocyte damage is usually used as an indicator when evaluating the progression and severity of DN in the clinic [8, 9]. Therefore, therapies that protect podocytes are considered to have great significance in the treatment of DN. However, the exact mechanism underlying podocyte injury and death in DN remains ambiguous.

Pyroptosis is a newly discovered cell death pathway that has been shown to play a critical role in AKI [10]. Pyroptosis initiated by the noncanonical inflammasome pathway is characterized by the activation of caspase-11 in mice and caspase-4 in humans and the cleavage of gasdermin D (GSDMD) [11]. GSDMD is a universal substrate for inflammatory caspases that plays a specific role in inflammatory caspase-initiated pyroptosis [12]. As a downstream effector of multiple inflammasomes, GSDMD is hydrolyzed by activated inflammatory caspases, and then the released N-terminus of GSDMD (GSDMD-N) translocates to the cell membrane [13]. Polymerization of GSDMD-N forms pores with a diameter of 20–30 nm [14]. Influx of extracellular substances and leakage of intracellular components initiate pyroptosis. DN is also considered to be an inflammatory disease [15]. Activation of inflammation has been observed in the development and progression of DN [16]. However, the involvement of pyroptosis in DN has not been studied.

Here, we provide evidence that caspase-11/4 and GSDMD-dependent pyroptosis is activated and contributes to podocyte loss and injury in DN.

MATERIALS AND METHODS

Materials

Basic RPMI-1640 medium and fetal bovine serum (FBS) were obtained from Gibco (Grand Island, NY, USA). Anti-caspase-11 (ab240991), anti-caspase-4 (ab25898), anti-GSDMD (ab219800), and anti-IL-18 (ab207323) were purchased from Abcam (Cambridge, MA, USA). Anti-GSDMD (sc-393656) and anti-β-actin (sc-8432) were purchased from Santa Cruz Biotechnology (Dallas, TX,

[1]Department of Physiology and Pathophysiology, School of Basic Medical Sciences, Shanghai Medical College, Fudan University, Shanghai 200032, China
Correspondence: Jun Liu (junliu@shmu.edu.cn) or Li-min Lu (lulimin@shmu.edu.cn)

Received: 15 January 2020 Accepted: 3 September 2020
Published online: 23 September 2020

UAS). Anti-IL-1β (NP-000567) was purchased from R&D (Minneapolis, MN, USA). Anti-p-NF-κB p65 (AF2006) was purchased from Affinity Biosciences (Changzhou, China). Anti-F4/80 (70076) was purchased from Cell Signaling Technology (Danvers, MA, USA).

Animals

Male C57BL/6J mice (20–25 g) were purchased from Shanghai SLAC Laboratory Animal Co., Ltd. (Shanghai, China). *Casp-11*$^{-/-}$ mice were obtained from the Jackson Laboratory (Bar Harbor, ME). *GSDMD*$^{-/-}$ mice were obtained from the Model Animal Research Center of Nanjing University (Jiangsu, China). Mice were housed in a specific pathogen-free facility. All animal experiments were performed following the Criteria of the Medical Laboratory Animal Administrative Committee of Shanghai and the Guide for Care and Use of Laboratory Animals of Fudan University. The protocols were approved by the Ethics Committee for Experimental Research, Shanghai Medical College, Fudan University (document number for animal use approval: 20160225-087).

Mouse models

High-fat diet (HFD)/streptozotocin (STZ)-induced diabetic mice were established by unilateral nephrectomy after feeding a HFD for 4 weeks. Two weeks after surgery, WT mice, *Casp-11*$^{-/-}$ mice and *GSDMD*$^{-/-}$ mice were induced to become diabetic by intraperitoneal injection of STZ (70 mg/kg body weight, freshly dissolved in 0.05 mol/L sterile sodium citrate, pH 4.5) for 3 consecutive days. Five days after the last STZ injection, the animals with a plasma glucose level above 16.7 mmol/mL were considered successful model animals and recruited into the experiment. The HFD/STZ-induced animals were fed a HFD for 12 weeks as described in previous studies. All mice had unrestricted access to food and water. Normal diet-fed mice were used as nondiabetic controls.

Cell culture

Human and mouse podocytes provided by Shandong University were cultured in RPMI-1640 medium as previously described. Cells were maintained in a quiescent state by culture in medium containing 0.5% FBS for 24 h before treatment. High-glucose (HG) treatment was performed by incubating cells in medium with a final glucose concentration of 30 mmol/L.

Immunohistochemistry and immunofluorescence

Renal sections were deparaffinized, rehydrated, and then subjected to antigen retrieval in 0.01 M citrate buffer (pH 6.0) with gentle shaking. After blocking with 5% bovine serum albumin, the sections were incubated with an anti-caspase-11 anti-GSDMD or anti-F4/80 antibody at 4 °C overnight, followed by incubation with a secondary antibody (Jackson Immuno Research Laboratories, West Grove, PA) at room temperature for 2 h. Fluorescence signals were viewed under a fluorescence microscope (Leica, Wetzlar, Germany).

Transmission electron microscopy (TEM)

Renal tissue samples were fixed in 2.5% glutaraldehyde. Then, they were washed in PBS (0.01 M) and postfixed with 1% osmium tetroxide. After gradient dehydration in acetone, the tissue samples were embedded in Araldite M (Sigma Aldrich, St. Louis, MO, USA). Ultrathin sections were cut using an ultramicrotome (Leica, Wetzlar, Germany) and stained with uranyl acetate and lead citrate. The sections were examined with a transmission electron microscope (H-7700, Hitachi, Japan).

Blood and urine examinations

The blood glucose level, urine samples, and body weight were evaluated every 4 weeks for 12 weeks. The blood glucose level in tail vein blood was measured. Urine samples were collected for 24 h in a metabolic cage. The urinary creatinine levels and urinary albumin concentration were measured, and the results are expressed as the urinary albumin/creatinine ratio (UACR).

ELISA

IL-1β and IL-18 concentrations in cell culture supernatants and blood were detected with commercial enzyme-linked immunosorbent assay kits (RayBiotech, Peachtree Corners, GA). The procedures were carried out according to the manufacturer's instructions.

Western blot analysis

Total tissue protein (30 μg) extracted from mouse kidneys was separated by 8%–12% SDS-PAGE and electrophoretically transferred to polyvinylidene difluoride membranes. The membranes were blocked with 5% skim milk for 30 min and incubated for 2 h with specific primary antibodies at room temperature. Immunoreactive bands were detected using HRP-conjugated goat anti-rabbit or goat anti-mouse IgG as the secondary antibody (1:5000, Santa Cruz Biotechnology Dallas, TX, USA).

Renal histology

Kidneys were fixed in 10% formalin and embedded in paraffin. Renal tissue samples were cut into 4-μm-thick sections. The sections were then dewaxed in xylene, rehydrated in decreasing concentrations of ethanol and washed in PBS three times for 10 min each time. Endogenous peroxidase activity was quenched for 45 min in a 0.6% methanol solution. After rewashing in PBS, the sections were blocked with 1% bovine serum albumin supplemented with avidin and a biotin blocking solution for 30 min. The sections were then stained with periodic acid-Schiff stain (PAS). Histological changes were observed at 400× optical magnification.

Caspase-11- and GSDMD-specific siRNAs

Caspase-11- and GSDMD-specific siRNAs were designed and synthesized by RiboBio Company (Guangzhou, Guangdong, China). A nonsilencing siRNA oligonucleotide that did not recognize any known homolog of mammalian genes was used as a negative control. Human podocytes were transfected with caspase-11-specific siRNA (50 nmol/L), GSDMD-specific siRNA (50 nmol/L) or control siRNA (50 nmol/L) using Lipofectamine 2000 Reagent (Invitrogen, Carlsbad, CA, USA) according to the manufacturer's instructions. Cells were treated with HG 48 h after siRNA transfection.

Statistical analysis

Data are shown as the mean ± SEM and were analyzed with SPSS version 19.0 (IBM Corp., Armonk, NY, USA). Column graphs were drawn by using GraphPad Prism version 6.0 (San Diego, CA, USA). Intergroup comparisons were conducted by Student's *t* test (2 groups) or one-way analysis of variance with post hoc analysis using Tukey's test as appropriate. A P value ≤ 0.05 was considered statistically significant.

RESULTS

Caspase-11 level was elevated in HFD/STZ-induced diabetic mice, and knockout of caspase-11 attenuated inflammation

Compared with those of normal diet-fed mice, the kidneys of HFD/STZ-induced diabetic mice exhibited significantly increased caspase-11 levels (Fig. 1a). PAS staining showed that compared with normal diet-fed mice, HFD/STZ-induced mice exhibited glomerular mesangium expansion and extracellular matrix deposition. Immunohistochemical staining showed that the expression of caspase-11 was rarely detected in normal diet-fed mice, while the positive staining signals for caspase-11 were significantly

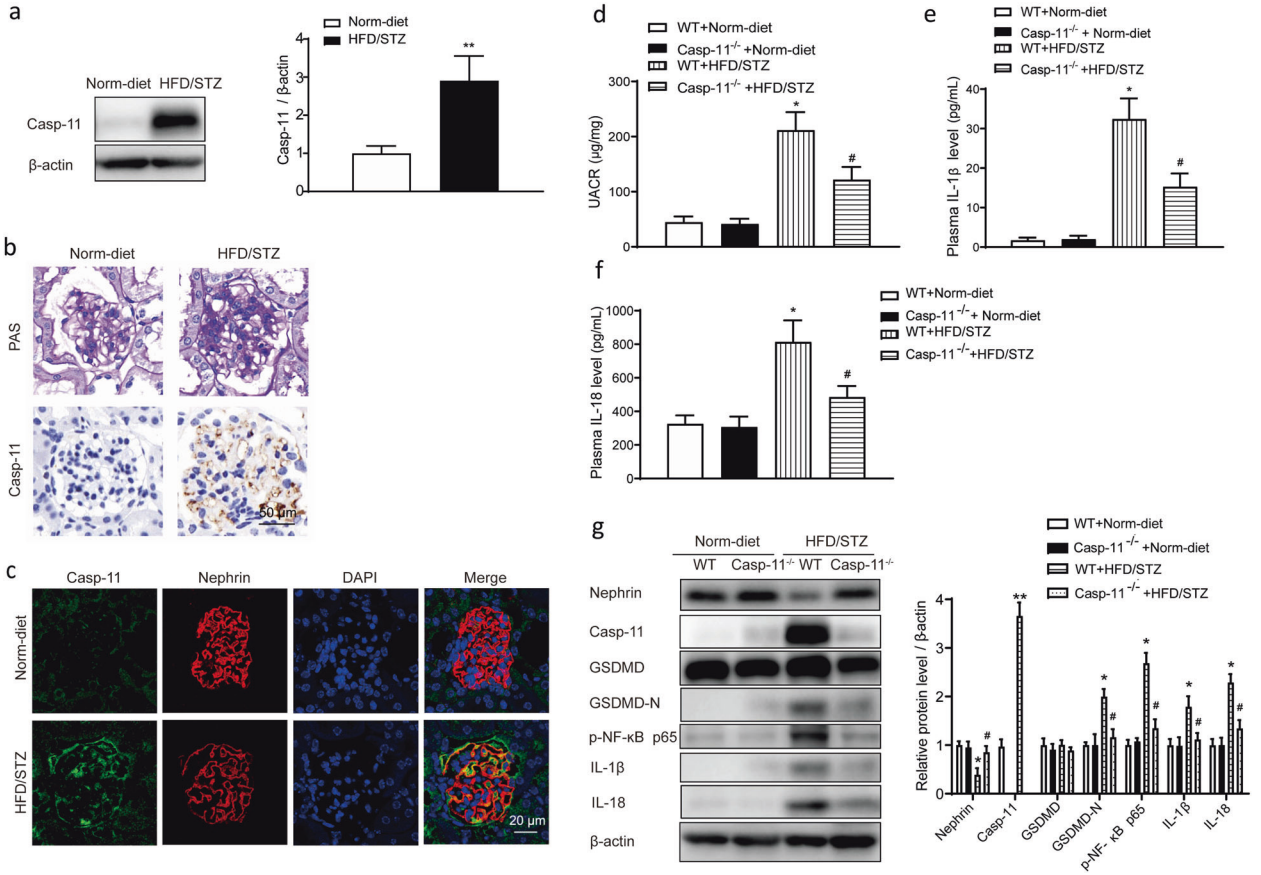

Fig. 1 Caspase-11 expression was elevated in HFD/STZ-induced mice and associated with inflammation. a Representative Western blot gel images and summary data showing the relative protein level of caspase-11 in the kidneys of control and HFD/STZ-induced mice. $^{**}P < 0.01$ versus normal diet-fed WT mice. All values are presented as the mean ± SEM ($n = 6$). **b** Photomicrographs showing typical glomerular structure changes and caspase-11 expression in the kidneys of normal diet-fed and HFD/STZ-induced mice. Original magnification, 400×. Scale bar, 50 μm. **c** Immunofluorescence staining image of caspase-11 and nephrin in normal diet-fed and HFD/STZ-induced mice. Original magnification, 200×. Scale bar, 20 μm. Measurements of the UACR (**d**) and serum IL-1β (**e**) and IL-18 levels (**f**) of normal diet-fed and HFD/STZ-induced mice. All values are presented as the mean ± SEM ($n = 6$). $^{*}P < 0.05$ compared with normal diet-fed mice. $^{\#}P < 0.05$ compared with HFD/STZ-induced WT mice. **g** Representative Western blot gel images and summary data showing the levels of nephrin, caspase-11, GSDMD, GSDMD-N, p-NF-κB p65, IL-1β, and IL-18 in renal lysates from different groups of mice ($n = 6$). $^{*}P < 0.05$ compared with normal diet-fed WT mice. $^{**}P < 0.01$ compared with normal diet-fed WT mice. $^{\#}P < 0.05$ compared with HFD/STZ-induced WT mice. WT wild type, Norm-diet normal diet, HFD high-fat diet, STZ streptozotocin, UACR urinary albumin to creatinine ratio.

increased in HFD/STZ-induced mice (Fig. 1b). Immunofluorescence results showed that caspase-11 was colocalized with the podocyte marker nephrin and that caspase-11 expression was significantly increased in the kidneys of HFD/STZ-induced mice (Fig. 1c). To determine the role of caspase-11 in HFD/STZ-induced diabetic mice, caspase-11 knockout (*Casp-11*$^{-/-}$) mice were utilized in the experiment. As shown in Table 1, *Casp-11*$^{-/-}$ mice did not show obvious differences in body weight or plasma glucose levels compared with WT mice. HFD/STZ treatment induced a significant increase in plasma glucose levels in both WT and *Casp-11*$^{-/-}$ mice, and the plasma glucose level was not significantly different between HFD/STZ-treated WT mice and *Casp-11*$^{-/-}$ mice. The UACR, an important parameter used to identify kidney injury, did not show any difference between WT and *Casp-11*$^{-/-}$ mice but was significantly increased in HFD/STZ-treated mice. Compared with that in WT mice, the increase in the UACR in HFD/STZ-treated *Casp-11*$^{-/-}$ mice was significantly attenuated (Fig. 1d). ELISA results showed that plasma IL-1β and IL-18 levels were significantly increased in HFD/STZ-induced mice and the increase was blunted in HFD/STZ-induced *Casp-11*$^{-/-}$ mice (Fig. 1e, f). Western blot results showed that caspase-11 expression was not detected in *Casp-11*$^{-/-}$ mice and was hardly detectable in control mice but was significantly increased in HFD/STZ-induced mice. Compared with those in WT mice, the levels of GSDMD-N, p-NF-κB p65, IL-1β, and IL-18 in HFD/STZ-induced WT mice were significantly increased, while these changes were blunted in diabetic *Casp-11*$^{-/-}$ mice (Fig. 1g). These results suggested that the increase in caspase-11 expression in diabetic mice was related to renal functional decline and inflammation.

Table 1. Body weight and glucose of the experimental animals.

	Wild-type mice		*Casp-11*$^{-/-}$ mice	
	Normal diet	HFD/STZ	Normal diet	HFD/STZ
Body weight (g)	28.8 ± 5.2	22.4 ± 4.8*	29.3 ± 3.6	24.2 ± 3.3*
Glucose (mmol/L)	6.6 ± 0.7	24.6 ± 5.9*	6.9 ± 0.5	25.9 ± 4.6*

Mice were fed a HFD for 4 weeks and then injected with 3 consecutive days of STZ (intraperitoneal at 70 mg/kg) followed by continued HFD feeding for an additional 12 weeks. Values are means ± SEM ($n = 6$).
HFD high-fat diet, *STZ* streptozotocin.
$^{*}P < 0.05$ versus normal-diet mice.

Knockout of caspase-11 attenuates podocyte loss and macrophage cell infiltration in HFD/STZ-induced diabetic mice

Histological analysis showed that HFD/STZ-induced mice exhibited increases in extracellular matrix accumulation, cell proliferation and glomerular hypertrophy compared with normal diet-fed mice. All these changes were significantly ameliorated in HFD/STZ-induced *Casp-11*$^{-/-}$ mice (Fig. 2a). TEM results showed that compared with normal diet-fed mice, HFD/STZ-induced mice exhibited podocyte foot process loss and fusion and these changes were also significantly ameliorated in HFD/STZ-induced *Casp-11*$^{-/-}$ mice (Fig. 2b). Immunohistochemistry results showed that F4/80^{+} cell numbers were increased in HFD/STZ-induced mice but reduced in HFD/STZ-induced *Casp-11*$^{-/-}$ mice, which indicated that macrophage infiltration was increased in diabetic mice and blunted by caspase-11 knockout (Fig. 2c). Immunofluorescence results showed that nephrin expression was decreased in HFD/STZ-induced mice and the decrease was partially reversed by caspase-11 knockout (Fig. 2d).

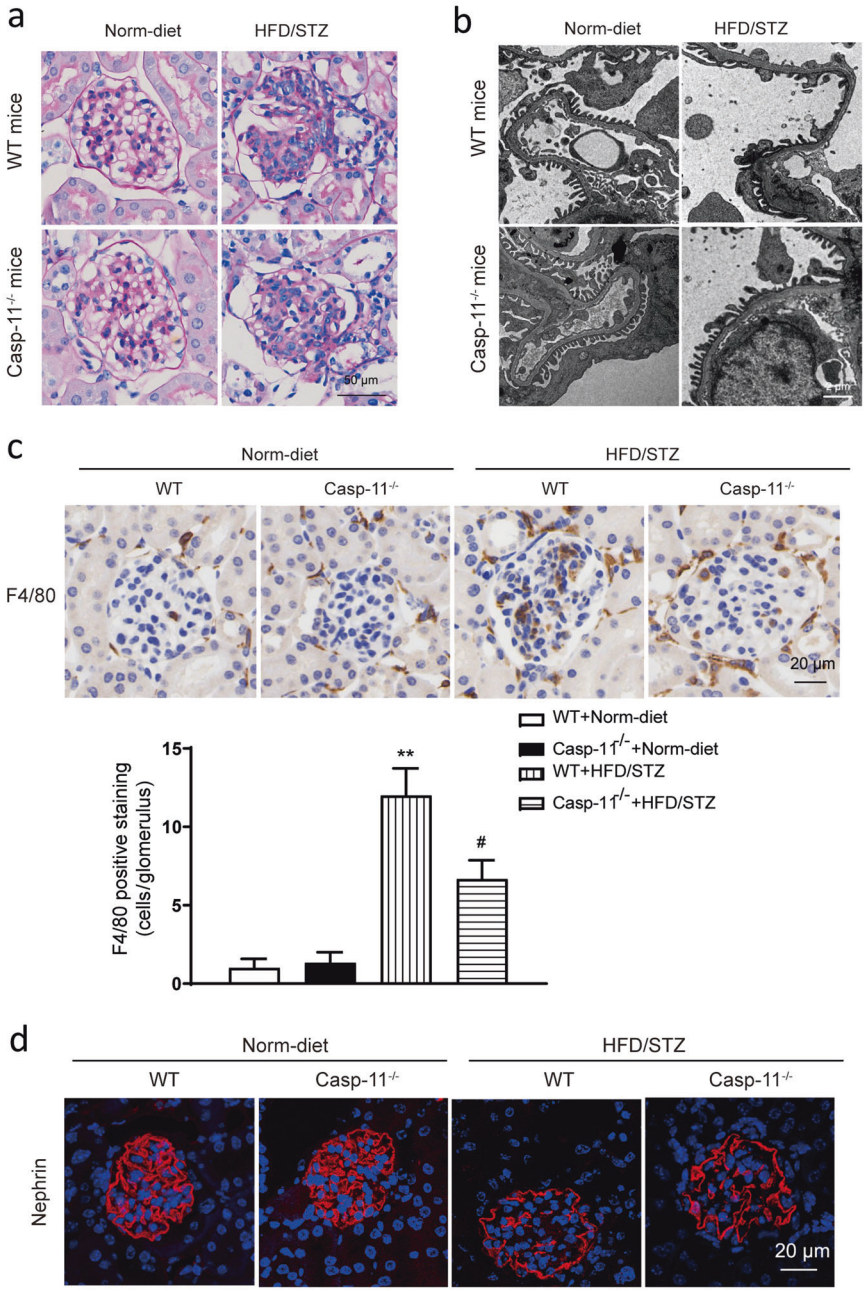

Fig. 2 Knockout of caspase-11 alleviated glomerular morphological changes in HFD/STZ-induced mice. a Representative photomicrographs of histological changes in glomeruli stained with PAS. Original magnification, 400×. Scale bar, 50 μm. **b** Representative photomicrographs of the podocyte foot process under transmission electron microscopy. Scale bar, 2 μm. **c** Representative photomicrographs of immunohistochemistry results showing the staining of F4/80^{+} macrophages in different groups. Original magnification, 400×. Scale bar, 20 μm. **d** Representative photomicrographs of immunofluorescence results showing the expression of nephrin in renal glomeruli in different groups of mice. Scale bar, 20 μm. WT wild type, Norm-diet normal diet, HFD high-fat diet, STZ streptozotocin. $^{**}P < 0.01$ vs WT + Norm-diet. $^{\#}P < 0.05$ vs WT + HFD/STZ.

Caspase-4 level was increased in high glucose-treated podocytes

Caspase-4 is the homolog of caspase-11 in humans. In cultured human podocytes, HG treatment significantly increased caspase-4 expression. In addition, the levels of nephrin and podocin, podocyte-specific markers, were reduced by HG treatment (Fig. 3a). Enzyme-linked immunosorbent assay results showed that the concentration of IL-1β in culture medium was significantly increased by HG treatment. Knockdown of caspase-4 expression by siRNA attenuated the increase in the IL-1β level (Fig. 3b). Western blot results showed that the protein levels of p-NF-κB p65, IL-1β, and IL-18 in cell lysates were also significantly increased after HG treatment and these changes were suppressed by knockdown of caspase-4 expression using siRNA. Knockdown of caspase-4 expression also partially reversed the HG-induced decrease in the nephrin level (Fig. 3c).

Cleavage of GSDMD and release of IL-1β were increased in HG-treated podocytes

As a major substrate of caspase-11/4, GSDMD was observed to be cleaved in cultured podocytes after HG treatment. As shown in Fig. 4a, HG treatment significantly increased the cleavage of GSDMD, which was indicated by a significant increase in the GSDMD-N level in HG-treated human podocytes. In addition, the levels of the podocyte markers nephrin and podocin were reduced. Mannitol, an osmotic control, did not influence these changes significantly (Fig. 4a). Enzyme-linked immunosorbent

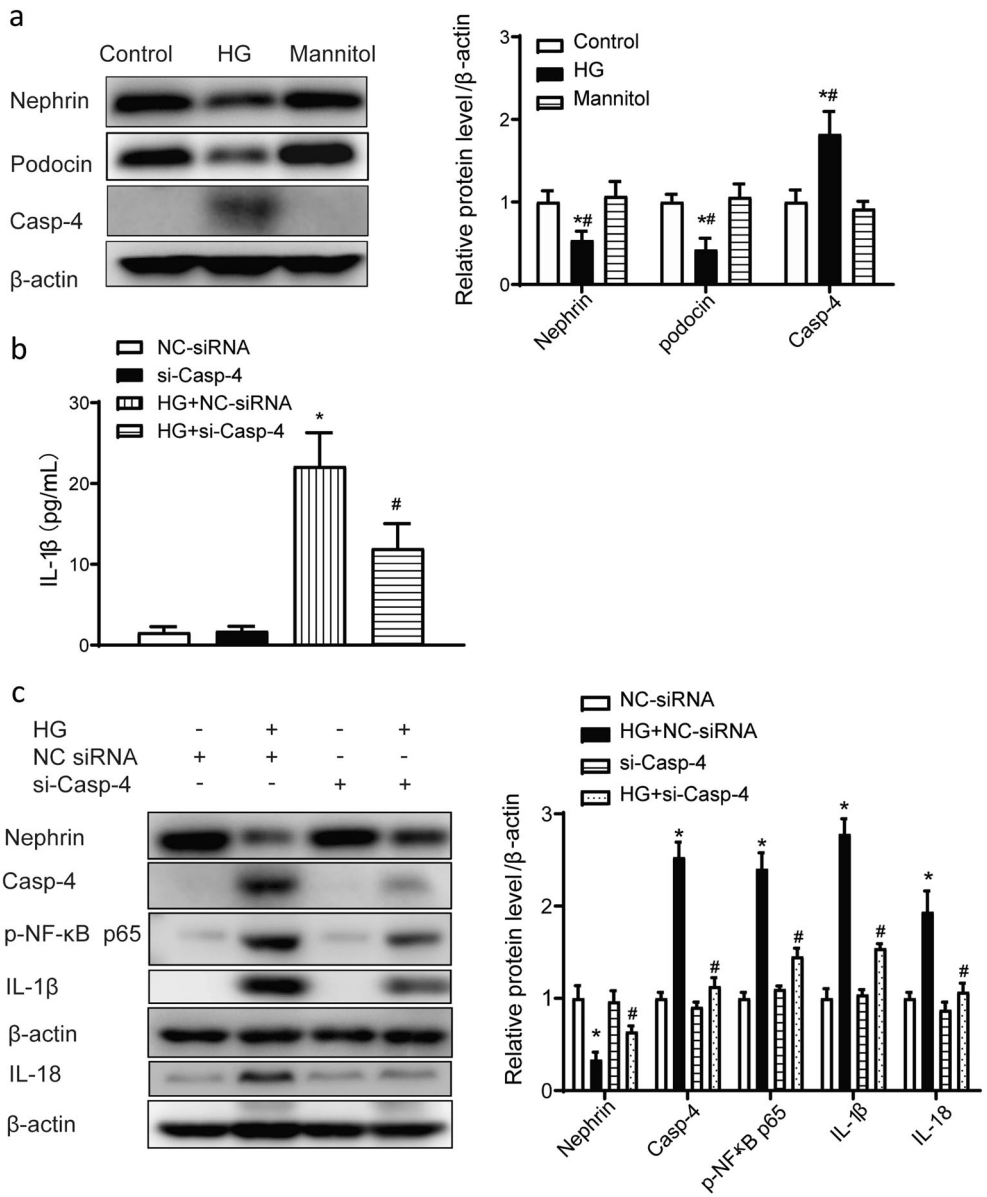

Fig. 3 High glucose-induced caspase-4 promoted the release of IL-1β in cultured human podocytes. a Representative Western blot gel images and summary data showing the levels of nephrin, podocin, and caspase-4 in podocytes from different groups. Data are presented as the mean ± SEM ($n = 6$). $^{*}P < 0.05$ versus control cells. $^{\#}P < 0.05$ versus mannitol. **b** Human podocytes were transfected with Casp-4-specific siRNA (50 nmol/L) or NC-siRNA (50 nmol/L) for 48 h and then treated with high glucose (30 μmol/L) for 24 h. ELISA analysis of IL-1β levels in culture medium. $^{*}P < 0.05$ versus NC-siRNA. $^{\#}P < 0.05$ versus HG + NC-siRNA. **c** Representative Western blot gel images and summary data showing the levels of p-NF-κB p65, IL-1β, and IL-18 after high-glucose treatment with or without caspase-4 knockdown by small interfering RNA. Data are presented as the mean ± SEM ($n = 6$). $^{*}P < 0.05$ versus NC-siRNA. $^{\#}P < 0.05$ versus HG + NC-siRNA. HG high glucose, NC negative control, siRNA small interfering RNA, ELISA enzyme-linked immunosorbent assay.

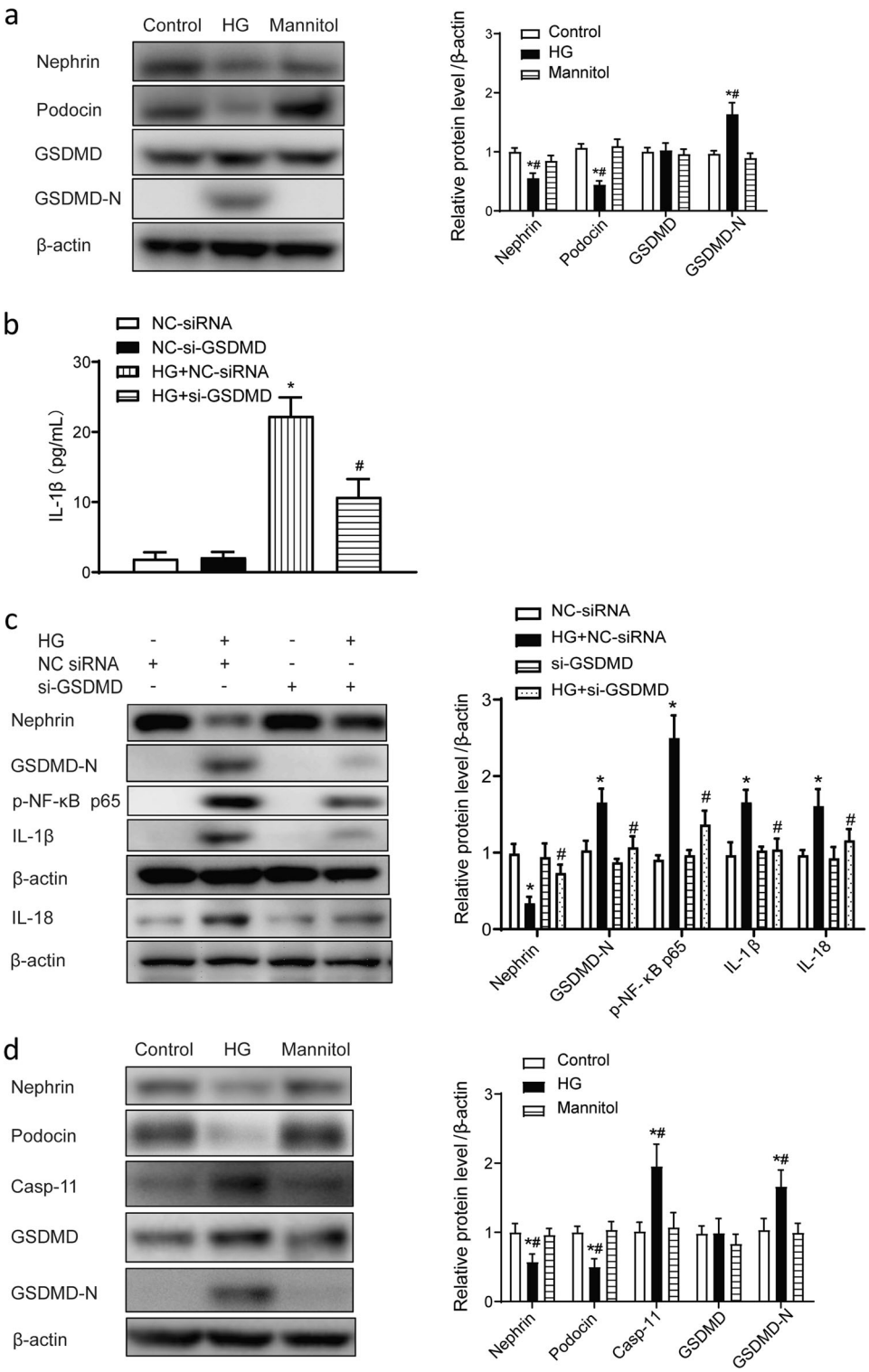

Fig. 4 GSDMD promoted the release of IL-1β in human podocytes in vitro. a Representative Western blot gel images and summary data showing the levels of nephrin, podocin, GSDMD, and GSDMD-N in human podocytes from different groups. Data are presented as the mean ± SEM ($n = 6$). *$P < 0.05$ versus control cells. #$P < 0.05$ versus mannitol. **b** Human podocytes were transfected with GSDMD-specific siRNA (50 nmol/L) or NC-siRNA (50 nmol/L) for 48 h and then treated with high glucose (30 μmol/L) for 24 h. ELISA analysis of IL-1β levels in culture medium. *$P < 0.05$ versus NC-siRNA. #$P < 0.05$ versus HG + NC-siRNA. **c** Representative Western blot gel images and summary data showing the levels of p-NF-κB p65, IL-1β, and IL-18 after high-glucose treatment with or without caspase-4 knockdown by small interfering RNA. Data are presented as the mean ± SEM ($n = 6$). *$P < 0.05$ versus NC-siRNA. #$P < 0.05$ versus HG + NC-siRNA. **d** Representative Western blot gel images and summary data showing the levels of nephrin, podocin, caspase-11, GSDMD, and GSDMD-N in mouse podocytes from different groups. Data are presented as the mean ± SEM ($n = 6$). *$P < 0.05$ versus control cells. #$P < 0.05$ versus mannitol. HG high glucose, NC negative control, siRNA small interfering RNA, ELISA enzyme-linked immunosorbent assay.

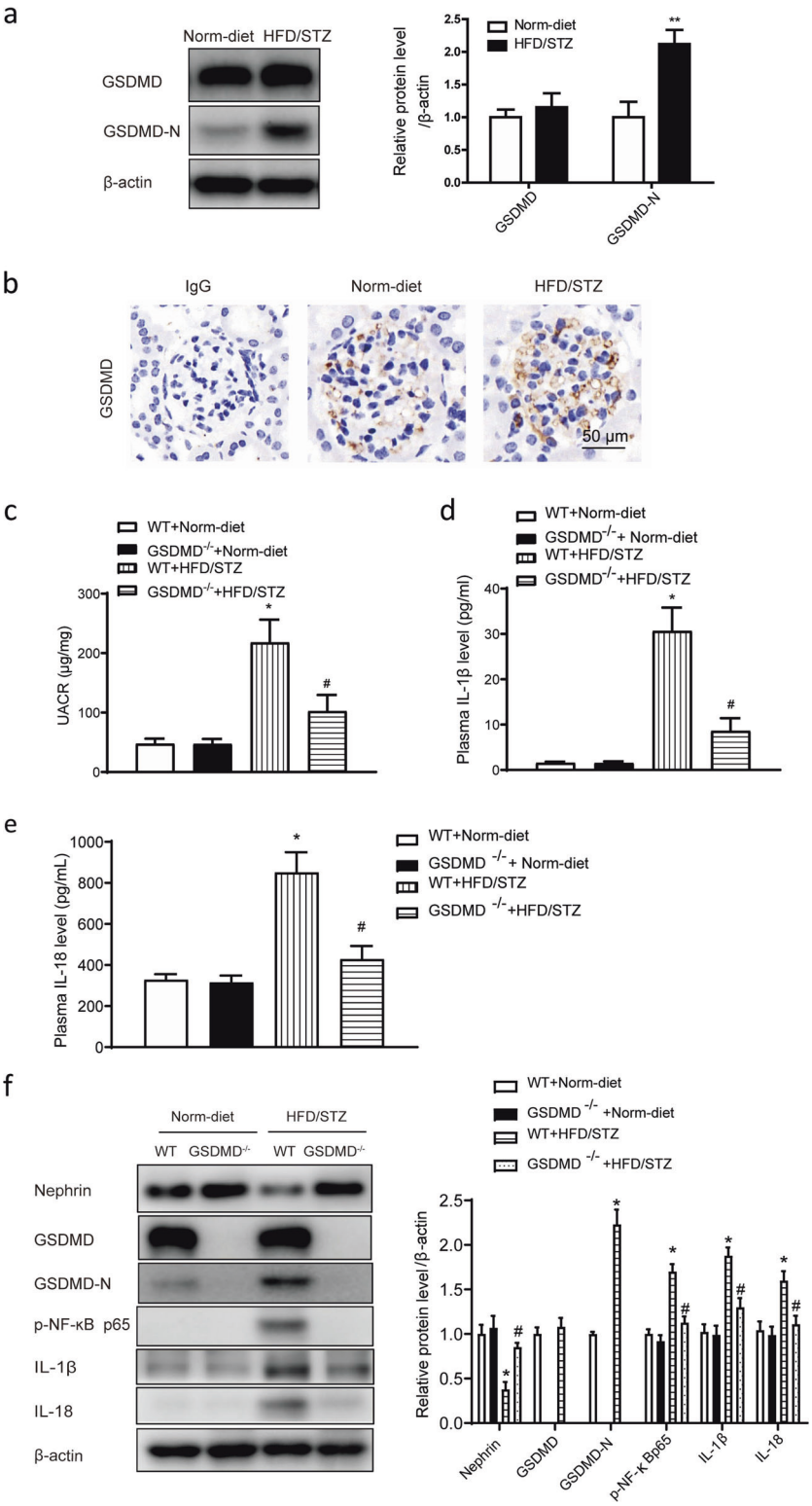

Fig. 5 The cleavage of GSDMD was elevated in HFD/STZ-induced diabetic mice and associated with inflammation. a Representative Western blot gel images and summary data showing the relative protein levels of GSDMD and GSDMD-N in the kidneys of HFD/STZ-induced mice. $^{**}P < 0.01$ versus normal diet-fed WT mice. All values are presented as the mean ± SEM ($n = 6$). **b** Immunohistochemical staining showing positive staining signals for GSDMD in glomeruli in both normal diet-fed and HFD/STZ-induced mice. Original magnification, 400×. Scale bar, 50 μm. Measurements of the UACR (**c**) and serum IL-1β (**d**) and IL-18 levels (**e**) in normal diet-fed and HFD/STZ-induced mice. All values are presented as the mean ± SEM ($n = 6$). $^{*}P < 0.05$ compared with normal diet-fed mice. $^{\#}P < 0.05$ compared with HFD/STZ-induced WT mice. **f** Representative Western blot gel images and summary data showing the levels of GSDMD, p-NF-κB p65, IL-1β, and IL-18 in renal lysates from different groups of mice ($n = 6$). $^{*}P < 0.05$ compared with normal diet-fed WT mice. $^{\#}P < 0.05$ compared with HFD/STZ-induced WT mice. WT wild type, Norm-diet normal diet, HFD high-fat diet, STZ streptozotocin, UACR urinary albumin to creatinine ratio.

assay results showed that the concentration of IL-1β was increased in the culture medium of HG-treated podocytes, while knockdown of GSDMD expression by siRNA blunted the increase in the IL-1β level in the medium (Fig. 4b). Western blot data showed that p-NF-κB p65, IL-1β, and IL-18 levels were significantly increased in HG-treated podocytes and knockdown of GSDMD expression significantly attenuated the increases in the p-NF-κB p65, IL-1β, and IL-18 levels after HG treatment (Fig. 4c). To further confirm the effects of HG on podocytes, mouse podocytes were also included in the experiment. Similar to the results observed with human podocytes, HG treatment increased the expression of caspase-11 and cleavage of GSDMD and downregulated nephrin and podocin expression (Fig. 4d).

Cleavage of GSDMD was elevated in HFD/STZ-induced mice and related to renal functional deterioration and inflammation

The expression and cleavage of GSDMD were also observed in HFD/STZ-induced diabetic mice. The results showed that the GSDMD-N level was significantly increased in the kidneys of HFD/STZ-induced mice compared with those of normal diet-fed mice, although the total GSDMD level did not show an obvious increase (Fig. 5a). Immunohistochemical staining showed that positive staining for GSDMD was visible in glomeruli in both normal diet-fed and HFD/STZ-induced mice (Fig. 5b). To determine the role of GSDMD cleavage in HFD/STZ-induced mice, GSDMD knockout (*GSDMD*$^{-/-}$) mice were included in the experiment. As shown in Table 2, compared with WT expression, GSDMD knockout did not influence body weight or plasma glucose levels. HFD/STZ treatment induced a significant increase in the plasma glucose level in both WT and *GSDMD*$^{-/-}$ mice. The plasma glucose level did not show a significant difference between HFD/STZ-treated WT mice and *GSDMD*$^{-/-}$ mice. The UACR also did not show any difference between WT and *GSDMD*$^{-/-}$ mice but was significantly increased in HFD/STZ-treated mice, and the increase in the UACR was significantly attenuated in HFD/STZ-induced GSDMD$^{-/-}$ mice (Fig. 5c). ELISA results showed that the plasma IL-1β and IL-18 levels changed in a similar pattern, as they were significantly increased in HFD/STZ-induced mice and the increases were blunted in HFD/STZ-induced *GSDMD*$^{-/-}$ mice (Fig. 5d, e). Western blot results showed that GSDMD-N expression was not detected in *GSDMD*$^{-/-}$ mice and was hardly detectable in WT mice but was significantly increased in HFD/STZ-induced mice. Compared with WT mice, HFD/STZ-induced mice exhibited significantly increased GSDMD-N, p-NF-κB p65, IL-1β, and IL-18 levels, and these changes were blunted in HFD/STZ-induced *GSDMD*$^{-/-}$ mice (Fig. 5f).

Knockout of GSDMD attenuated podocyte injury in HFD/STZ-induced diabetic mice

Histological analysis showed that compared with normal diet-fed mice, HFD/STZ-induced mice exhibited increases in glomerular matrix accumulation, cell proliferation and hypertrophy, and all these changes were significantly ameliorated in HFD/STZ-induced *GSDMD*$^{-/-}$ mice (Fig. 6a). TEM results showed the compared with normal diet-fed mice, HFD/STZ-induced mice exhibited loss or fusion of podocyte foot processes (Fig. 6b), and these changes were significantly ameliorated in HFD/STZ-induced *GSDMD*$^{-/-}$ mice. Immunohistochemistry results showed that F4/80^{+} cell numbers were increased in HFD/STZ-induced mice compared with normal diet-fed mice and GSDMD knockout reduced the HFD/STZ-induced increase in F4/80^{+} cell numbers, which indicated that macrophage infiltration was increased in diabetic mice and that the increase in macrophage infiltration was blunted by GSDMD knockout (Fig. 6c). Immunofluorescence results showed that compared with that in normal diet-fed mice, the expression of nephrin in HFD/STZ-induced mice was decreased and the change was significantly ameliorated in HFD/STZ-induced *GSDMD*$^{-/-}$ mice (Fig. 6d).

Table 2. Body weight and glucose of the experimental animals.

	Wild-type mice		*GSDMD*$^{-/-}$ mice	
	Normal diet	HFD/STZ	Normal diet	HFD/STZ
Body weight (g)	29.2 ± 4.2	22.4 ± 3.2*	29.3 ± 2.0	24.3 ± 3.3*
Glucose (mmol/L)	6.7 ± 0.3	24.1 ± 4.1*	6.1 ± 0.6	24.7 ± 6.4*

Mice were fed a HFD for 4 weeks and then injected with 3 consecutive days of STZ (intraperitoneal at 70 mg/kg) followed by continued HFD feeding for an additional 12 weeks. Values are means ± SEM ($n = 6$).
HFD high-fat diet, *STZ* streptozotocin.
*$P < 0.05$ versus normal-diet mice.

DISCUSSION

DN has become an important pathogenic factor in the development of chronic kidney disease as the incidence of diabetes has rapidly increased [17, 18]. The exact mechanism of DN has not been fully elucidated, although a large number of studies have been performed in recent decades [19]. A widely accepted opinion on the development of DN is that DN is a comprehensive consequence of injuries to multiple renal targets under hyperglycemic conditions [20, 21]. Among those targets, podocytes are well accepted as an early injury site since proteinuria is a typical incipient symptom of DN.

In a previous study, an increase in podocyte apoptosis was reported and considered the reason for the excessive loss of podocytes. However, a novel form of cell death, pyroptosis, was recently elucidated [22]. Pyroptosis is defined as immunogenic cell death with some characteristics of programmed cell death. Pyroptosis has been identified in some pathological changes in the kidneys [23, 24]. Therefore, it is necessary to clarify whether pyroptosis is implicated in the loss of podocytes in DN.

In this study, our results showed that the expression of caspase-11 was increased in diabetic mice. At the same time, the cleavage of GSDMD was also increased. In cultured human and mouse podocytes, high glucose levels stimulated the expression of caspase-4/11 and cleavage of GSDMD. These results suggest that caspase-11/4 and GSDMD-dependent pyroptosis is initiated under hyperglycemic conditions. Using *Casp-11*$^{-/-}$ or *GSDMD*$^{-/-}$mice, our study showed that knockout of either caspase-11 or GSDMD significantly ameliorated renal functional deterioration and morphological changes in glomeruli and podocytes, which suggests that caspase-11/4 and GSDMD-dependent pyroptosis is implicated in the development of DN.

Chronic activation of inflammation is another feature of DN [25, 26]. Activation of inflammation is associated with renal functional deterioration and scar formation [16]. In this experiment, inflammatory cytokine production was elevated in diabetic mice, which is consistent with previous observations [27, 28]. Knockout of caspase-11 or GSDMD suppressed the elevations in inflammatory cytokine levels, which suggests that the activation of pyroptosis, an immunogenic cell death process, is associated with the activation of inflammation. In a sense, the result also suggests that pyroptosis is associated, at least in part, with the activation of inflammation in DN.

In this study, global caspase-11 or GSDMD knockout mice were used. Therefore, a limitation of this study was that we could not rule out the possibility that the beneficial effect might also be derived from a reduction in endothelial cell and tubular epithelial cell damage [29, 30].

In summary, our results demonstrate for the first time that the caspase-11/4 and GSDMD-dependent pathway is implicated in podocyte injury and loss in DN. Suppression of pyroptosis may protect the development of DN by preventing podocyte loss and local inflammation activation.

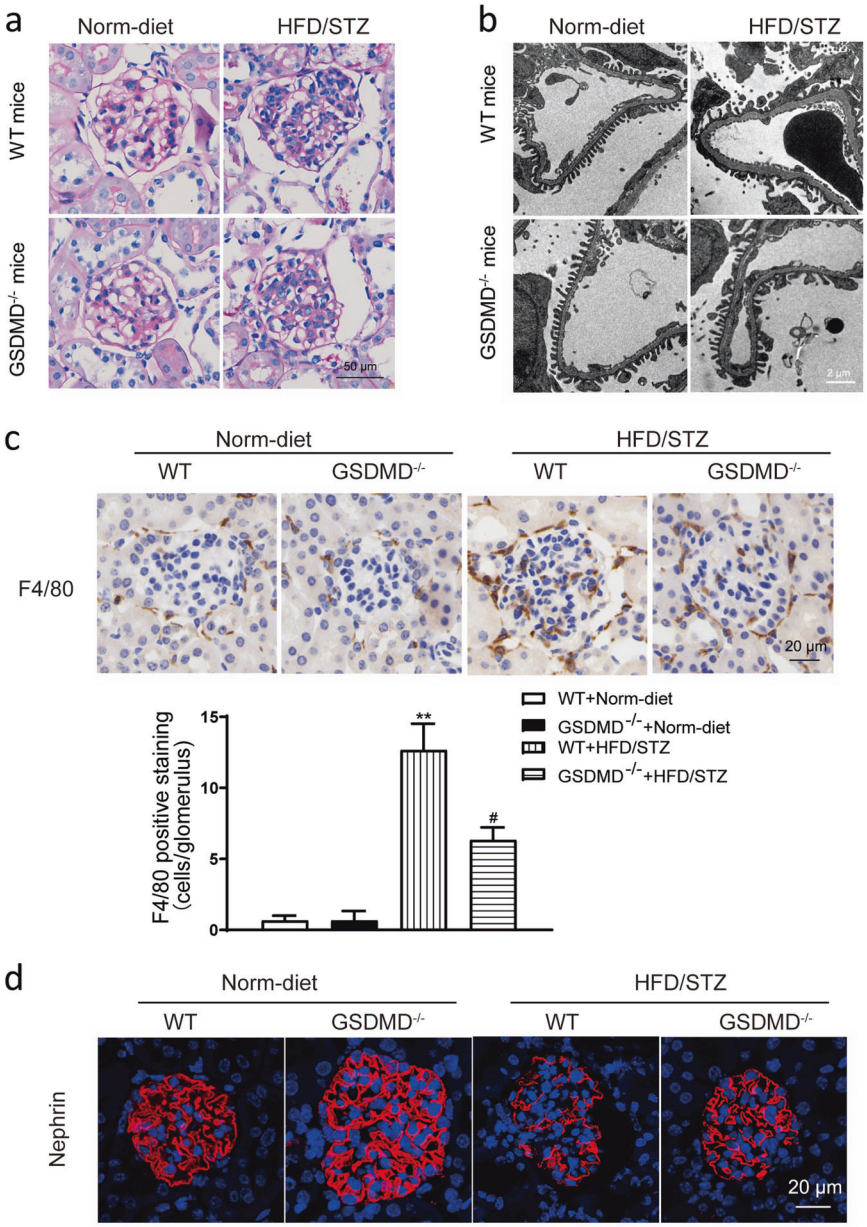

Fig. 6 Knockout of GSDMD alleviated podocyte injury in HFD/STZ-induced mice. a Representative photomicrographs of histological changes in glomeruli stained with PAS. Original magnification, 400×. Scale bar, 50 μm. **b** Representative photomicrographs of podocyte foot processes in different groups of mice generated by transmission electron microscopy. Scale bar, 2 μm. **c** Representative photomicrographs of immunohistochemistry results showing the staining of F4/80^{+} macrophages in different groups of mice. Original magnification, 400×. Scale bar, 20 μm. **d** Representative photomicrographs of immunofluorescence results showing the expression of nephrin in glomeruli in different groups of mice. Scale bar, 20 μm. WT wild type, Norm-diet normal diet, HFD high-fat diet, STZ streptozotocin. $^{**}P < 0.01$ vs WT + Norm-diet. $^{\#}P < 0.05$ vs WT + HFD/STZ.

ACKNOWLEDGEMENTS

This research was financially supported by the Natural National Science Foundation of China (No. 81873603, 81670664, 81470591) to LL and the Science and Technology Commission of Shanghai Municipality (14DZ2260200, the project of Shanghai Key Laboratory of Kidney and Blood Purification).

AUTHOR CONTRIBUTIONS

QC, JL, and LML conceived and designed the study, and drafted the manuscript; QC and JP performed the experiments. QC analyzed the data; QC, JP, FY, HYX, PPC, JYL, PQZ, ZL, and WZ participated in designing the study and revising the manuscript. All authors read and approved the manuscript.

ADDITIONAL INFORMATION

Competing interests: The authors declare no competing interests.

REFERENCES

1. Gnudi L, Coward R, Long DA. Diabetic nephropathy: perspective on novel molecular mechanisms. Trends Endocrinol Metab. 2016;27:820–30.
2. Maezawa Y, Takemoto M, Yokote K. Cell biology of diabetic nephropathy: roles of endothelial cells, tubulointerstitial cells and podocytes. J Diabetes Investig. 2015;6:3–15.
3. Pichaiwong W, Hudkins KL, Wietecha T, Nguyen TQ, Tachaudomdach C, Li W, et al. Reversibility of structural and functional damage in a model of advanced diabetic nephropathy. J Am Soc Nephrol. 2013;24:1088–102.

4. Wang X, Liu J, Zhen J, Zhang C, Wan Q, Liu G, et al. Histone deacetylase 4 selectively contributes to podocyte injury in diabetic nephropathy. Kidney Int. 2014;86:712–25.
5. Liu M, Liang K, Zhen J, Zhou M, Wang X, Wang Z, et al. Sirt6 deficiency exacerbates podocyte injury and proteinuria through targeting Notch signalin. Nat Commun. 2017;8:413.
6. Dai H, Liu Q, Liu B. Research progress on mechanism of podocyte depletion in diabetic nephropathy. J Diabetes Res. 2017;2017:2615286.
7. Nishad R, Mukhi D, Tahaseen SV, Mungamuri SK, Pasupulati AK. Growth hormone induces Notch1 signaling in podocytes and contributes to proteinuria in diabetic nephropathy. J Biol Chem. 2019;294:16109–22.
8. Motonishi S, Nangaku M, Wada T, Ishimoto Y, Ohse T, Matsusaka T, et al. Sirtuin1 maintains actin cytoskeleton by deacetylation of cortactin in injured podocytes. J Am Soc Nephrol. 2015;26:1939–59.
9. He Y, Zhang M, Wu Y, Jiang H, Fu H, Cai Y, et al. Aberrant activation of Notch-1 signaling inhibits podocyte restoration after islet transplantation in a rat model of diabetic nephropathy. Cell Death Dis. 2018;9:10.
10. Li Y, Xia W, Wu M, Yin J, Wang Q, Li S. et al. Activation of GSDMD contributes to acute kidney injury induced by cisplatin. Am J Physiol Renal Physiol. 2020;318: F96–106.
11. Shi J, Zhao Y, Wang K, Shi X, Wang Y, Huang H, et al. Cleavage of GSDMD by inflammatory caspases determines pyroptotic cell death. Nature. 2015;526:660–5.
12. Ding J, Wang K, Liu W, She Y, Sun Q, Shi J, et al. Pore-forming activity and structural autoinhibition of the gasdermin family. Nature. 2016;535:111–6.
13. Aglietti RA, Estevez A, Gupta A, Ramirez MG, Liu PS, Kayagaki N, et al. GsdmD p30 elicited by caspase-11 during pyroptosis forms pores in membranes. Proc Natl Acad Sci U S A. 2016;113:7858–63.
14. Khanova Elena, Wu Raymond, Wang Wen, Yan Rui, Chen Yibu, French SamuelW, et al. Pyroptosis by caspase11/4-gasdermin-D pathway in alcoholic hepatitis in mice and patients. Hepatology. 2018;67:1737–53.
15. Yaribeygi H, Katsiki N, Butler AE, Sahebkar A. Effects of antidiabetic drugs on NLRP3 inflammasome activity, with a focus on diabetic kidneys. Drug Discov Today. 2019;24:256–62.
16. Shahzad K, Bock F, Dong W, Wang H, Kopf S, Kohli S, et al. Nlrp3-inflammasome activation in non-myeloid-derived cells aggravates diabetic nephropathy. Kidney Int. 2015;87:74–84.
17. Chaplin S. Qtern: DPP-4 and SGLT2 inhibitor combination for type 2 diabetes. Prescriber. 2017;28:47–9.
18. You H, Gao T, Raup-Konsavage WM, Cooper TK, Bronson SK, Reeves WB, et al. Podocyte-specific chemokine (C-C motif) receptor 2 overexpression mediates diabetic renal injury in mice. Kidney Int. 2017;91:671–82.
19. Raz I, Cernea S, Cahn A. SGLT2 inhibitors for primary prevention of cardiovascular events. J Diabetes. 2020;12:5–7.
20. Abais JM, Zhang C, Xia M, Liu Q, TWB Gehr, Boini KM, et al. NADPH oxidase-mediated triggering of inflammasome activation in mouse podocytes and glomeruli during hyperhomocysteinemia. Antioxid Redox Sign. 2013;18: 1537–48.
21. Zhou L, Liu Y. Wnt/beta-catenin signalling and podocyte dysfunction in proteinuric kidney disease. Nat Rev Nephrol. 2015;11:535–45.
22. Zhang C, Boini KM, Xia M, Abais JM, Li X, Liu Q, et al. Activation of nod-like receptor protein 3 inflammasomes turns on podocyte injury and glomerular sclerosis in hyperhomocysteinemia. Hypertension. 2012;60:154–62.
23. Xu B, Jiang M, Chu Y, Wang W, Chen D, Li X, et al. Gasdermin D plays a key role as a pyroptosis executor of non-alcoholic steatohepatitis in humans and mice. J Hepatol. 2018;68:773–82.
24. Miao N, Yin F, Xie H, Wang Y, Xu Y, Shen Y, et al. The cleavage of gasdermin D by caspase-11 promotes tubular epithelial cell pyroptosis and urinary IL-18 excretion in acute kidney injury. Kidney Int. 2019;96:1105–20.
25. Vandanmagsar B, Youm Y, Ravussin A, Galgani JE, Stadler K, Mynatt RL, et al. The NLRP3 inflammasome instigates obesity-induced inflammation and insulin resistance. Nat Med. 2011;17:179–88.
26. Zhang Z, Sun L, Wang Y, Ning G, Minto AW, Kong J, et al. Renoprotective role of the vitamin D receptor in diabetic nephropathy. Kidney Int. 2008;73: 163–71.
27. Kim S, Lee S, Kim Y, Kim S, Seo J, Choi Y, et al. Hyperuricemia-induced NLRP3 activation of macrophages contributes to the progression of diabetic nephropathy. Am J Physiol Renal Physiol. 2015;308:F993–1003.
28. Wang C, Pan Y, Zhang Q, Wang F, Kong L. Quercetin and allopurinol ameliorate kidney injury in STZ-treated rats with regulation of renal NLRP3 inflammasome activation and lipid accumulation. PLoS One. 2012;7:e38285.
29. Wang Y, Zhu X, Yuan S, Wen S, Liu X, Wang C, et al. TLR4/NF-κB signaling induces GSDMD-related pyroptosis in tubular cells in diabetic kidney disease. FrontEndocrinol. 2019;10:603.
30. Gu J, Huang W, Zhang W, Zhao T, Gao C, Gan W, et al. Sodium butyrate alleviates high-glucose-induced renal glomerular endothelial cells damage via inhibiting pyroptosis. Int Immunopharmacol. 2019;75:105832.